Front propagation in anomalous diffusive media governed by time-fractional diffusion

Andrea Mentrelli[a,b], Gianni Pagnini[b,c]

[a] *Department of Mathematics & CIRAM, University of Bologna, via Saragozza 8, 40123 Bologna, Italy*
[b] *BCAM – Basque Center for Applied Mathematics, Alameda de Mazarredo 14, 48009 Bilbao, Basque Country – Spain*
[c] *Ikerbasque – Basque Foundation for Science, Alameda Urquijo 36-5, Plaza Bizkaia, 48011 Bilbao, Basque Country – Spain*

Abstract

When a front propagates into a medium characterized by an underlying random diffusive process, the front motion becomes random. The random motion of interface particles is here assumed to be governed by the multidimensional time-fractional diffusion. In particular, the average position of particles, and then of the interface, is assumed to be tracked by the Level Set Method (LSM) while the spreading of interface particles around the average position is described by a probability density function (PDF) that characterizes the diffusion into the underlying random environment. The effective average front emerges to be determined by the superposition of the solutions of the ordinary LSM weighted by a distance function which corresponds to the particle PDF. Analytical and numerical results are shown and discussed.

Keywords: random front propagation, Level Set Method, multidimensional time-fractional diffusion, M-Wright/Mainardi function

2010 MSC: 60G22, 60K37, 35F21, 65M08

Email addresses: andrea.mentrelli@unibo.it (Andrea Mentrelli), gpagnini@bcamath.org (Gianni Pagnini)

1. Introduction

Front propagation is of interest in several fields of applied sciences. However, in many applications the front is embedded into a random environment and therefore it gets a random motion. Moreover, when a random motion occurs into a complex media it is often characterized by anomalous diffusion [1, 2, 3, 4]. The aim of the present research is to suggest and investigate the suitability and the properties of an approach to track fronts with a random motion that is characterized by anomalous diffusion. This approach was first proposed to model the burned mass fraction in turbulent premixed combustion [5] and it has been recently applied to wildland fire propagation [6, 7, 8, 9].

The interface is assumed to be embodied by particles with random motion. The average position of particles, and then of the interface, is assumed to be tracked by the Level Set Method (LSM) [10] while the spreading of interface particles around the average position is described by a probability density function (PDF) that characterizes the diffusion into the underlying random environment. The effective average front emerges to be determined by the superposition of the solutions of the ordinary LSM weighted by a distance function which corresponds to the particle PDF. The anomalous diffusion is modelled by the multidimensional time-fractional diffusion equation. It is well known that Green's function of one-dimensional time-fractional diffusion equation is related to the M-Wright/Mainardi function [11, 12, 13]. By using a subordination-type formula of the M-Wright/Mainardi function [14] that is based on one-dimensional Gaussian PDF, it is shown that Green's function for multidimensional cases can be represented by the same subordination-type formula involving multidimensional Gaussian PDF. This simplifies existing representation of multidimensional Green's fucntion [15].

The LSM [16, 10] is one of the most widely used and successful tools for tracking fronts and it has been adopted in many different problems, including, for example, turbulent premixed combustion (involving the so-called G-equation) [17], wildland fire propagation [18], groundwater infiltration [19], biology [20]

and material science [21]. It is a highly robust and accurate method for tracking interfaces in any spatial dimension. The motion of the propagating surface is governed by Hamilton–Jacobi equations and a noteworthy property of LSM is that it can be used in the same basic formulation for problems with any spatial dimension. The Hamilton–Jacobi equations of the LSM can be derived by three ways [10]. In particular, within the analysis view, the interface is defined as an isoline of an auxiliary function so that the total derivative of the selected isosurface corresponds to the motion of the interface. Such isoline of the auxiliary function is refereed to as level set function. In this setting, sharp gradients and cusps can be easily accounted for and the effects of curvature may be easily incorporated. Then the LSM is particularly useful to handle problems in which the speed of the evolving interface is dependent on the interface properties, such as curvature and normal direction, as well as on the boundary conditions at the interface location. Hence, it is suitable for problems in which the topology of the evolving interface changes during the events, as well as when topological merging and breaking naturally occur.

The formulation chosen for the present study being based on the LSM has the same striking property to be compatible with every type of geometry and flow in a simple and versatile way, and it emerges to be easily modifiable to include more detailed and correct physics. Moreover, it should be remarked here that this approach avoids to assume fluctuations of the level set function, see also [22], as indeed it is assumed in other literature approaches [23, 24, 25, 26] even if it is not correct because the level set function being an isosurface has a constant value and fluctuations are zero by definition. But the position of the isoline is random and it fluctuates.

The formalism of this approach can be re-arranged to be compared with the Smoothed Particle Hydrodynamics (SPH) [27], a well established and numerical robust approach for many practical problems as fluid-structure interactions. However, the characteristic problems of the SPH, namely the choice of the kernel function and of the smoothing length, are here avoided because they

are straightforwardly determined by the particle PDF. This can be considered a positive feature of the present approach.

This approach compares also with two widely used literature approaches for turbulent premixed combustion, namely the LSM/G-equation [17] and the Zimont balance equation [28]. Hence, its original formulation [5] physically substantiates both the LSM/G-equation and the Zimont combustion models. It is here reminded that the G-equation is related to the celebrated Kardar–Parisi–Zhang equation for growing interfaces [29] and that Zimont model is also known in the literature as Turbulent Flame Closure model [30].

Furthermore, the present approach compares also with the Stochastic Level Set Method (SLSM) adopted in computer vision. Typical problems in computer vision consist in recovering a certain surface or region through a shape optimization framework. However, classical methods suffer from being sometimes stuck in local minima. A method has been developed which considers a stochastic motion and the LSM [31, 32, 33]. The SLSM is used to overcome the stuck problem coupled with a decision mechanism. The SLSM is quite close to the approach here proposed for what concerns the picture of the process. In fact, in both cases, the interface is assumed to be driven by the level set equation but with a random speed. However, the final aims are strongly different and so the mathematical construction. In fact, in computer vision problems the final aim is not to compute the average shape after a large number of independent realizations, but to recover a certain shape with the frontline and a proper stochastic differential equation is derived. In the present study, the interest is indeed focused on the average properties of the processes for applications in physics and engineering. Even if it could be possible to have average properties of the process obtained with the SLSM by performing the ensemble average of many independent realizations, the approach here proposed uses physical arguments to derive the PDF of the interface particle displacement. Hence, the present approach overcomes the problem to establish the correct stochastic differential equations. It provides directly the shape of the effective average front line on the

basis of physical arguments. Then it can be understood as the averaged counterpart of the method adopted in computer vision. Under the physical point of view, it seems to be much more confident and sound to introduce the PDF of interface particles, which is reasonably available from data, then to establish the stochastic differential equations for the SLSM. Notwithstanding this strong difference in the mathematical formulation, the deep discussion developed in computer vision is an important guideline for future derivation of stochastic models within the proposed approach.

The present study extends to multidimensional cases a preliminary study realized by the authors [34]. The paper is organized as follows. In Section 2 the main features of the proposed approach to track front embedded into a random environment are described. The adopted approach is based in the LSM and the PDF of displacement of interface particles. Dispersion of interface particles is assumed to be governed by time-fractional diffusion equation, and solutions of the latter in one–, two– and three–dimensional cases are analyzed in Section 3. In particular a new representation based on the Gaussian PDF is shown for Green's functions. In Section 4 the numerical methodology adopted for the calculation of Green's functions and the propagation of the effective average front is introduced. In Section 5 numerical results concerning two-dimensional front propagation are presented and discussed. Finally, conclusions are drawn in Section 6 and future developments are outlined.

2. Tracking method for random fronts

Consider a propagating interface composed by a sufficiently large number of particles with random motion. Let $\mathbf{X}^{\omega}(t, \overline{\mathbf{x}}_0)$ be the trajectory of each particle with the same fixed initial condition $\mathbf{X}^{\omega}(0, \overline{\mathbf{x}}_0) = \overline{\mathbf{x}}_0$ in any realization indexed by ω. By using statistical mechanics formalism [35], the trajectory of a single interface particle is marked out by the one-particle density function $p_{\mathrm{d}}^{\omega}(\mathbf{x}; t) = \delta(\mathbf{x} - \mathbf{X}^{\omega}(t, \overline{\mathbf{x}}_0))$, where $\delta(\mathbf{x})$ is the Dirac δ-function and d represents the spatial dimension. The evolution of the average trajectory $\overline{\mathbf{x}}(t)$ is

obtained uniquely by a deterministic time-reversible map. If the number of particles embodying the interface is assumed to be constant while the frontline enlarges, an incompressibility-like condition follows and the Jacobian J of the average motion law is $J = d\overline{\mathbf{x}}_0/d\overline{\mathbf{x}} = 1$. In terms of particle trajectories it holds $\mathbf{X}^\omega(t, \overline{\mathbf{x}}_0) \to \mathbf{X}^\omega(t, \overline{\mathbf{x}})$. Denoting by $\langle\cdot\rangle$ the ensemble average, the PDF of the displacement of the interface particles around the average position $\overline{\mathbf{x}}$ is $p_{\mathrm{d}}(\mathbf{x}; t|\overline{\mathbf{x}}) = \langle\delta(\mathbf{x} - \mathbf{X}^\omega(t, \overline{\mathbf{x}}))\rangle$.

Let Γ be a simple closed surface, or an ensemble of simple non-intersecting closed surfaces, that represents the propagating interface under consideration and let Ω be the region bounded by Γ. In the case of an interface Γ made of more than one closed surface, the domain Ω is not simply connected, resulting in more than one bounded areas independently evolving. Moreover, let $\gamma : \mathcal{S} \times [0, +\infty[\to \mathbb{R}$ be a function defined on the domain of interest $\mathcal{S} \subseteq \mathbb{R}^d$ such that the level set $\gamma(\mathbf{x}, t) = \gamma_*$ coincides with the evolving front, i.e. $\Gamma(t) = \{\mathbf{x} \in \mathcal{S} \mid \gamma(\mathbf{x}, t) = \gamma_*\}$. In the case of Γ being an ensemble of n surfaces, the ensemble of the n interfaces is considered as *interface*.

The deterministic level set function $\gamma(\mathbf{x}, t)$ may be written as

$$\gamma(\mathbf{x}, t) = \int_{\mathcal{S}} \gamma(\overline{\mathbf{x}}, t)\ \delta(\mathbf{x} - \overline{\mathbf{x}})\ d\overline{\mathbf{x}}. \tag{1}$$

Let $\gamma^\omega(\mathbf{x}, t)$ be the random level set function corresponding the ω-realization that embeds the random frontline Γ^ω, then the analog of (1) reads

$$\gamma^\omega(\mathbf{x}, t) = \int_{\mathcal{S}} \gamma(\overline{\mathbf{x}}, t)\ \delta(\mathbf{x} - \mathbf{X}^\omega(t, \overline{\mathbf{x}}))\ d\overline{\mathbf{x}}\,. \tag{2}$$

The subsets of the domain $\mathcal{S}$ corresponding to the interface Γ and to the region Ω enclosed by Γ (which represent, respectively, the interface and the domain bounded by it) may be conveniently identified as the positive-valued regions selected by the two indicator functions $\mathcal{I}_\Gamma$, $\mathcal{I}_\Omega : \mathcal{S} \times [0, +\infty[\to \{0, 1\}$ defined as follows:

$$\mathcal{I}_\Gamma(\mathbf{x}, t) = \begin{cases} 1\,, & \text{if} \quad \gamma(\mathbf{x}, \mathrm{t}) = \gamma_* \\ \\ 0\,, & \text{elsewhere} \end{cases}, \tag{3}$$

and

$$\mathcal{I}_\Omega(\mathbf{x},t) = \begin{cases} 1\,, & \text{if} \quad \gamma\,(\mathbf{x},\mathrm{t}) \leq \gamma_* \\ \\ 0\,, & \text{elsewhere} \end{cases} . \tag{4}$$

The indicator functions at time $t = 0$, i.e. $\mathcal{I}_\Gamma(\mathbf{x}, t = 0)$ and $\mathcal{I}_\Omega(\mathbf{x}, t = 0)$, are denoted in the following as $\mathcal{I}_{\Gamma_0}(\mathbf{x})$ and $\mathcal{I}_{\Omega_0}(\mathbf{x})$, respectively.

Accordingly to (2), $\mathcal{I}_\Gamma$ and $\mathcal{I}_\Omega$ are replaced by random indicator functions $\mathcal{I}_{\Gamma^\omega}, \mathcal{I}_{\Omega^\omega} : \mathcal{S} \times [0, +\infty[\to \{0, 1\}$ defined as follows:

$$\begin{aligned} \mathcal{I}_{\Gamma^\omega}(\mathbf{x},t) &= \int_{\mathcal{S}} \mathcal{I}_{\Gamma_0}(\overline{\mathbf{x}}_0)\, \delta(\mathbf{x} - \mathbf{X}^\omega(t,\overline{\mathbf{x}}_0))\, d\overline{\mathbf{x}}_0 \\ &= \int_{\Gamma_0} \delta(\mathbf{x} - \mathbf{X}^\omega(t,\overline{\mathbf{x}}_0))\, d\overline{\mathbf{x}}_0 \\ &= \int_{\Gamma(t)} \delta(\mathbf{x} - \mathbf{X}^\omega(t,\overline{\mathbf{x}}))\, d\overline{\mathbf{x}} \end{aligned} \tag{5}$$

and

$$\begin{aligned} \mathcal{I}_{\Omega^\omega}(\mathbf{x},t) &= \int_{\mathcal{S}} \mathcal{I}_{\Omega_0}(\overline{\mathbf{x}}_0)\, \delta(\mathbf{x} - \mathbf{X}^\omega(t,\overline{\mathbf{x}}_0))\, d\overline{\mathbf{x}}_0 \\ &= \int_{\Omega_0} \delta(\mathbf{x} - \mathbf{X}^\omega(t,\overline{\mathbf{x}}_0))\, d\overline{\mathbf{x}}_0 \\ &= \int_{\Omega(t)} \delta(\mathbf{x} - \mathbf{X}^\omega(t,\overline{\mathbf{x}}))\, d\overline{\mathbf{x}}\,. \end{aligned} \tag{6}$$

Hence the *effective indicator* of the region surrounded by an random front, $\varphi_e(\mathbf{x}, t) : \mathcal{S} \times [0, +\infty[\to [0, 1]$, may be defined as:

$$\begin{aligned} \varphi_e(\mathbf{x},t) = \langle \mathcal{I}_{\Omega^\omega}(\mathbf{x},t) \rangle &= \langle \int_{\Omega(t)} \delta(\mathbf{x} - \mathbf{X}^\omega(t,\overline{\mathbf{x}}))\, d\overline{\mathbf{x}} \rangle \\ &= \int_{\Omega(t)} \langle \delta(\mathbf{x} - \mathbf{X}^\omega(t,\overline{\mathbf{x}})) \rangle\, d\overline{\mathbf{x}} \\ &= \int_{\Omega(t)} p_{\mathrm{d}}(\mathbf{x}; t|\overline{\mathbf{x}})\, d\overline{\mathbf{x}}\,. \end{aligned} \tag{7}$$

Equation (7) has been originally proposed to model the burned mass fraction in turbulent premixed combustion [5].

It should be noted that the *effective indicator* $\varphi_e(\mathbf{x}, t)$ is not an indicator function in the classical sense. Actually, by using terminology from fuzzy logic,

it is a *membership function*, its range being the compact interval $[0,1]$ rather than the discrete set $\{0,1\}$. Despite this, the concept of probability which led to equation (7) should not be confused with the concept of degree of truth (typical of fuzzy logic), then $\varphi_e(\mathbf{x},t)$ is classify as an indicator function. Since the range of the effective indicator $\varphi_e(\mathbf{x},t)$ is the compact interval $[0,1]$, a criterion to mark the *effective* surrounded region Ω_e has to be stated. In particular, region Ω_e is here marked when the effective indicator exceeds an arbitrarily fixed threshold value φ_e^{th}, i.e. $\Omega_e(t) = \{\mathbf{x} \in \mathcal{S} \mid \varphi_e(\mathbf{x},t) > \varphi_e^{th}\}$.

Making use of the indicator function $\mathcal{I}_\Omega$ defined in (4), equation (7) can be further written as:

$$\varphi_e(\mathbf{x},t) = \int_{\mathcal{S}} \mathcal{I}_\Omega(\overline{\mathbf{x}},t)\, p_{\mathrm{d}}(\mathbf{x};t|\overline{\mathbf{x}})\, d\overline{\mathbf{x}}\,. \tag{8}$$

In the deterministic case, i.e. $\mathbf{X}^\omega(t,\overline{\mathbf{x}}) = \overline{\mathbf{x}}(t)$ for all realizations, it turns out that $p_{\mathrm{d}}(\mathbf{x};t|\overline{\mathbf{x}}) = \delta(\mathbf{x} - \overline{\mathbf{x}}(t))$, and from equation (8) it is recovered $\varphi_e(\mathbf{x},t) = \mathcal{I}_\Omega(\mathbf{x},t)$. Formula (8) compares with the SPH [27], however, as stated in the Introduction, the choices of the kernel function and of the smoothing length are avoided because they are straightforwardly determined by the particle PDF $p_{\mathrm{d}}(\mathbf{x};t|\overline{\mathbf{x}})$.

Finally, indicator function $\mathcal{I}_\Omega(\overline{\mathbf{x}},t)$ marks the region $\Omega(t)$ that is bounded by an interface propagating according to the average trajectory $\overline{\mathbf{x}}(t)$. Region $\Omega(t)$ can be tracked by the LSM [10] and then, recalling the definition of $\mathcal{I}_\Omega(\overline{\mathbf{x}},t)$ in (4), the level set function $\gamma(\overline{\mathbf{x}},t)$ is governed by the following Hamilton–Jacobi equation

$$\frac{D\gamma}{Dt} = \frac{\partial\gamma}{\partial t} + \frac{d\overline{\mathbf{x}}}{dt}\cdot\nabla\gamma = 0\,, \quad \gamma(\overline{\mathbf{x}},\, t=0) = \gamma_0(\overline{\mathbf{x}})\,, \tag{9}$$

where γ_0 is the initial field embedding the interface Γ at $t=0$, $\Gamma_0 \equiv \Gamma(t=0)$. If the motion of the interface is aligned with the interface normal $\hat{\mathbf{n}} = -\nabla\gamma/\|\nabla\gamma\|$, it holds

$$\frac{d\overline{\mathbf{x}}}{dt} = \mathbf{V}(\overline{\mathbf{x}},t) = \mathcal{V}(\overline{\mathbf{x}},t)\,\hat{\mathbf{n}} \tag{10}$$

and equation (9) becomes

$$\frac{\partial\gamma}{\partial t} = \mathcal{V}(\overline{\mathbf{x}},t)\,\|\nabla\gamma\|\,, \tag{11}$$

which is the *ordinary* level set equation.

It is worth mentioning here that an alternative representation of the dynamics of the propagating front is possible whenever the normal velocity of the front $\mathcal{V}(\overline{\mathbf{x}}, t)$ is constant in time and stricly positive (or strictly negative). In this case, let $\tau(\overline{\mathbf{x}})$ be the *arrival time* function that represents the temporal instant at which the front reaches the point $\overline{\mathbf{x}}$, then $\|\nabla\tau\|$ is the rate of change of the arrival time with respect to the change in the front distance, i.e.

$$\|\nabla\tau\| = \frac{1}{\mathcal{V}}\,, \quad \tau(\overline{\mathbf{x}}) = 0 \quad \forall\overline{\mathbf{x}} \in \Gamma_0\,. \tag{12}$$

Equation (12) is known as eikonal equation and it is a time-independent version of the level set (Hamilton–Jacobi) equation (9). It has the important advantage of allowing – when applicable – to greatly reduce the computational effort required for solving the front tracking problem by solving a time-independent problem instead of a time-dependent one.

3. Multidimensional time-fractional diffusion equation

The PDF of interface particle displacement $p_{\mathrm{d}}(\mathbf{x}; t)$ is assumed to be governed by the d-dimensional time-fractional diffusion equation. Time-fractional diffusion equation is obtained from the classical diffusion equation by replacing the first order time derivative with a real order derivative operator [36, 37, 38, 39, 15, 40]. This replacement can be done by using the time fractional derivative operator in the Caputo sense or in the Riemann–Liouville sense. However, these two forms are equivalent if standard initial condition is used [41].

Let $0 < \beta \leq 1/2$ be a real positive parameter, then the time-fractional diffusion equation in the Caputo sense reads

$${}_*D_t^{2\beta} p_{\mathrm{d}} = \nu\,\nabla^2 p_{\mathrm{d}}\,, \quad p_{\mathrm{d}}(\mathbf{x}; 0) = \delta(\mathbf{x})\,, \tag{13}$$

where coefficient ν is a positive constant with dimensions $[\nu] = [L]^2[T]^{-2\beta}$ and ${}_*D_t^{\mu}$ is the *Caputo* fractional derivative that is defined by the Laplace transfor-

mation

$$\int_0^{+\infty} \mathrm{e}^{-st}\,\{{}_*D_t^{\mu}\,f(t)\}\,dt = s^{\mu}\,\widetilde{f}(s) - \sum_{k=0}^{m-1} s^{\mu-1-k}\,f^{(k)}(0^+)\,, \tag{14}$$

with $m-1 < \mu \leq m$ and $m \in N$, where $f(t)$ is a sufficiently well-behaved function $f(t)$ and $\widetilde{f}(s)$ its Laplace transform.

The time-fractional diffusion equation in the Riemann–Liouville sense reads

$$\frac{\partial p_{\mathrm{d}}}{\partial t} = \nu\, D_t^{1-2\beta}\,\nabla^2 p_{\mathrm{d}}\,, \quad p_{\mathrm{d}}(\mathbf{x};0) = \delta(\mathbf{x})\,, \tag{15}$$

where D_t^{μ} is the Riemann–Liouville fractional derivative defined as

$$\int_0^{+\infty} \mathrm{e}^{-st}\,\{D_t^{\mu}\,f(t)\}\,dt = s^{\mu}\,\widetilde{f}(s)\,, \tag{16}$$

provided that all the limiting values $f^{(k)}(0^+)$ are finite with $k \in N$ such that $0 \leq k \leq m-1$ where $m \in N$ and $m-1 < \mu \leq m$.

When $\beta = 1/2$, both equations (13) and (15) reduce to the classical diffusion equation

$$\frac{\partial p_{\mathrm{d}}}{\partial t} = \nu\,\nabla^2 p_{\mathrm{d}}\,, \quad p_{\mathrm{d}}(\mathbf{x};0) = \delta(\mathbf{x})\,. \tag{17}$$

Applying Laplace and Fourier transformations to (13), and analogously to (15), the fundamental solution, or Green's function, $p_{\mathrm{d}}(\mathbf{x};t)$ for arbitrary spatial dimension d follows to be [15]

$$p_{\mathrm{d}}(\mathbf{x};t) = \frac{1}{(2\pi)^{d+1}\,i}\int_{-i\infty}^{+i\infty}\left\{\int_{R^d}\frac{s^{2\beta-1}}{s^{2\beta}+\nu\kappa^2}\,\mathrm{e}^{i\mathbf{k}\cdot\mathbf{x}}\,d\mathbf{k}\right\}\mathrm{e}^{st}\,ds\,, \quad k = |\mathbf{k}|\,. \tag{18}$$

Solution of (18) is [15]

$$p_{\mathrm{d}}(\mathbf{x};t) = \frac{1}{(2\pi\sqrt{\nu})^{d/2+1}\,i}\int_{-i\infty}^{+i\infty} s^{\beta(d/2+1)-1}\,\mathrm{e}^{st}\,\mathcal{K}_{d/2-1}\left(\frac{s^{\beta}r}{\sqrt{\nu}}\right)ds\,, \quad r = |\mathbf{x}|\,, \tag{19}$$

where $\mathcal{K}_{\theta}$ is the Macdonald function, or modified Bessel function of the second kind, of order θ. Moreover, $p_{\mathrm{d}}(\mathbf{x};t)$ is real by setting $s = -i\xi$, $\xi \in \mathbb{R}$, and then $s^{\beta} = \mathrm{e}^{-i\pi\beta\,\mathrm{sgn}\,\xi/2}|\xi|^{\beta}$ [15].

However, a general representation of $p_{\mathrm{d}}(\mathbf{x};t)$ simpler than (19) can be obtained by using the following subordination type integral representation of the

M-Wright/Mainardi function [14]

$$M_{\eta/2}(x;t) = 2\int_0^{+\infty} \frac{\mathrm{e}^{-x^2/(4\tau)}}{\sqrt{4\pi\tau}}\, M_\eta\left(\frac{\tau}{t^\eta}\right)\frac{d\tau}{t^\eta}\,, \quad 0<\eta<1\,, \tag{20}$$

where $M_\eta(z)$, $0<\eta<1$, is represented by series as [37, 38, 11, 12]

$$M_\eta(z) = \sum_{n=0}^{\infty} \frac{(-z)^n}{n!\,\Gamma[-\eta n+(1-\nu)]} = \frac{1}{\pi}\sum_{n=1}^{\infty} \frac{(-z)^{n-1}}{(n-1)!}\,\Gamma(\eta n)\,\sin(\pi\eta n)\,. \tag{21}$$

For computational reasons, it is here reported that the Laplace transform of the M-Wright/Mainardi function is [39, 11, 12]

$$\int_0^{+\infty} \mathrm{e}^{-st} M_\eta(t)\,dt = E_\eta(-s)\,, \quad 0<\eta<1\,, \quad Re(s)>0\,, \tag{22}$$

where $E_\eta(z)$ is the Mittag–Leffler function defined by [42]

$$E_\rho(z) = \sum_{n=0}^{\infty} \frac{z^n}{\Gamma(\rho n+1)}\,, \quad \rho>0\,, \quad z\in C\,. \tag{23}$$

In view of its leading role in diffusive stochastic processes, the M-Wright/Mainardi function is now considered as a natural (fractional) generalization of the Gaussian function [13]. In this respect, it is here reported the following noteworthy particular case

$$M_{1/2}(z) = \frac{1}{\sqrt{\pi}}\,\exp\left(-z^2/4\right)\,. \tag{24}$$

Formula (20) can be extended to a general spatial dimension d as follows

$$M^d_{\eta/2}(\mathbf{x};t) = 2\int_0^{+\infty} \frac{\mathrm{e}^{-r^2/(4\tau)}}{(4\pi\tau)^{d/2}}\, M_\eta\left(\frac{\tau}{t^\eta}\right)\frac{d\tau}{t^\eta}\,, \quad r=|\mathbf{x}|\,, \quad 0<\eta<1\,, \tag{25}$$

and, by noting that $r^2=\sum_{i=1}^d x_i^2$, it can be rewritten as

$$M^d_{\eta/2}(\mathbf{x};t) = 2\int_0^{+\infty} \prod_{i=1}^{d} \frac{\mathrm{e}^{-x_i^2/(4\tau)}}{(4\pi\tau)^{1/2}}\, M_\eta\left(\frac{\tau}{t^\eta}\right)\frac{d\tau}{t^\eta}\,, \qquad 0<\eta<1\,. \tag{26}$$

When $d=1$, formulae (25) and (26) reduces to (20) and $M^1_\eta(z)=M_\eta(z)$, $0<\eta<1$, is the M-Wright/Mainardi function defined in (21). Since the following Laplace transform pair holds [39]

$$\int_0^{+\infty} \mathrm{e}^{-st} M_\eta\left(\frac{\tau}{t^\eta}\right)\frac{dt}{t^\eta} = s^{\eta-1}\mathrm{e}^{-\tau s^\eta}\,, \tag{27}$$

after application of Laplace and Fourier transformations to (26) it follows that

$$M^d_{\eta/2}(\mathbf{x};t) = 2\,\frac{1}{(2\pi)^{d+1}\,i}\,\int_{-i\infty}^{+i\infty}\left\{\int_{R^d}\left[\int_0^{+\infty}\prod_{i=1}^{d}\mathrm{e}^{-\tau k_i^2}\,\mathrm{e}^{-\tau s^\eta}\,d\tau\right]\,\mathrm{e}^{i\mathbf{k}\cdot\mathbf{x}}\,d\mathbf{k}\right\}\,s^{\eta-1}\mathrm{e}^{st}\,ds\,. \tag{28}$$

Hence, since $\sum_{i=1}^d k_i^2 = k^2$,

$$\begin{aligned} M^d_{\eta/2}(\mathbf{x};t) &= \frac{2}{(2\pi)^{d+1}\,i}\,\int_{-i\infty}^{+i\infty}\left\{\int_{R^d}\left[\int_0^{+\infty}\mathrm{e}^{-\tau(s^\eta+\nu k^2)}\,d\tau\right]\mathrm{e}^{i\mathbf{k}\cdot\mathbf{x}}\,d\mathbf{k}\right\}\,s^{\eta-1}\mathrm{e}^{st}\,ds \\ &= \frac{2}{(2\pi)^{d+1}\,i}\,\int_{-i\infty}^{+i\infty}\left\{\int_{R^d}\frac{s^{\eta-1}}{s^\eta+k^2}\,\mathrm{e}^{i\mathbf{k}\cdot\mathbf{x}}\,d\mathbf{k}\right\}\mathrm{e}^{st}\,ds\,, \end{aligned} \tag{29}$$

which compares with (18) suggests to rewrite $p_{\mathrm{d}}(\mathbf{x};t)$ as

$$p_{\mathrm{d}}(\mathbf{x};t) = \frac{1}{2\sqrt{\nu}}\,M^d_\beta\left(\frac{\mathbf{x}}{\sqrt{\nu}};t\right) = \int_0^{+\infty}\frac{\mathrm{e}^{-r^2/(4\nu\tau)}}{(4\pi\nu\tau)^{d/2}}\,M_{2\beta}\left(\frac{\tau}{t^{2\beta}}\right)\frac{d\tau}{t^{2\beta}}\,, \tag{30}$$

where the changes $k \to \sqrt{\nu}k$ and $\mathbf{x} \to \mathbf{x}/\sqrt{\nu}$ are done. Formula (30) is both analytically and numerically less cumbersome than (18).

In particular, from (30) the relation between $p_{1\mathrm{d}}(x;t)$ and $p_{3\mathrm{d}}(\mathbf{x};t)$ can be straightforwardly obtained [15]

$$p_{3\mathrm{d}}(\mathbf{x};t) = -\frac{1}{2\pi r}\,\frac{\partial}{\partial r}p_{1\mathrm{d}}(r;t)\,. \tag{31}$$

Constraint on parameter β guarantees to have a proper diffusion process characterized by an unimodal PDF [37, 39]. On the contrary, when $1/2 < \beta < 1$ function $M_\beta(z)$ is bimodal and no kind of diffusion corresponds to $p_{3\mathrm{d}}$ because it has also negative values. Subdiffusive character of diffusion is highlighted by particle variance that in one dimension is [39, 15]

$$\sigma^2_{1\mathrm{d}} = \int_{-\infty}^{+\infty}x^2\,p_{1\mathrm{d}}(x;t)\,dx = \frac{2}{\Gamma(2\beta+1)}\,\nu\,t^{2\beta}\,, \tag{32}$$

so that $\sigma^2_{2\mathrm{d}} = 2\,\sigma^2_{1\mathrm{d}}$ and $\sigma^2_{3\mathrm{d}} = 3\,\sigma^2_{1\mathrm{d}}$ [15].

4. Numerical approach

The evolution of random fronts propagating in subdiffusive and diffusive media has been numerically investigated by means of a software package developed

for this goal. The code makes use of a general-purpose library (`liblsm90`) which aims at providing a robust and efficient tool for tracking co-dimension one fronts propagating in one–, two– and three–dimensional media. The library, written in Fortran2008/OpenMP, is presently still under active development and is intended to be released as open source software under the GNU/GPLv2 licence [43]. Along with standard algorithms useful for the calculation of the front evolution by means of the classical LSM, the library includes Fast Marching Method (FMM) algorithms, which allow to efficiently solve the eikonal equation (12) arising from the classical LSM formulation in place of the standard Hamilton–Jacobi equation whenever it is possible, as in the case here under consideration.

The numerical evaluation of the M-Wright/Mainardi function $M_\eta(z)$ and of the fundamental solutions in d dimensions $p_d(\mathbf{x};t)$ have been performed by means of a python library (`pyMlib`) based on state-of-the-art algorithms for the Mittag–Leffler function [44] as well as on standard Laplace inversion and standard integration techniques available in the `Integrate` submodule of the `SciPy` scientific library.

All the results presented in the following have been obtained making use of the above-mentioned software and have been post-processed for exposition purposes by means of open source software such as `SciPy` [45] and `Matplotlib` [46] in the IPython framework [47].

All the calculations have been performed by means of the computational server available at the Basque Center for Applied Mathematics (BCAM) in Bilbao, Basque Country – Spain.

5. Numerical results

Numerical calculation of Green's functions of the multidimensional time-fractional diffusion equation (15) are presented in this section along with a selection of computational results concerning the propagation of fronts in sub-diffusive and diffusive media.

Except for the fundamental solutions, which are presented in Section 5.1 for the one–, two– and three–dimensional cases, any further discussion and numerical results of random front propagation presented in Section 5.2 are limited to the case of one–dimensional fronts propagating in two–dimensional media, the case of one–dimensional media being discussed elsewhere [34] and a thorough analysis including three–dimensional cases under development.

Once the main features of plane fronts propagating in one–dimensional media has been understood [34], the two–dimensional case has the relevant advantage of allowing to investigate the propagation of fronts in subdiffusive and diffusive media in practical situation of effective interest in which multidimensional effects possibly come into play, still avoiding the complexity of a three–dimensional analysis.

5.1. Fundamental solutions

In Figure 1, the fundamental solutions of the time-fractional diffusion equation (15) discussed in Section 3 are presented for the one–, two– and three–dimensional cases. For each of the three cases, the fundamental solutions are plotted for five different values of the parameter β, i.e. $\beta = 0.1$, 0.2, 0.3, 0.4 and 0.5, corresponding the latter to the case of ordinary diffusion and the other values to subdiffusive processes.

5.2. Random front propagation

The analysis proposed in this section concerns the investigation of random front propagation in two–dimensional subdiffusive and diffusive media, focusing on the effects of the diffusion coefficient ν, the parameter β and the velocity of the front $\mathcal{V}$ on the features of the random propagating fronts.

The case of an initial front profile with circular shape is first discussed, as to focus on the effects of ν, β and $\mathcal{V}$ avoiding the two–dimensional effects connected to a non-axisymmetric initial front profile. The two-dimensional effects are then discussed under the case of a square-shaped initial front profile, with the main

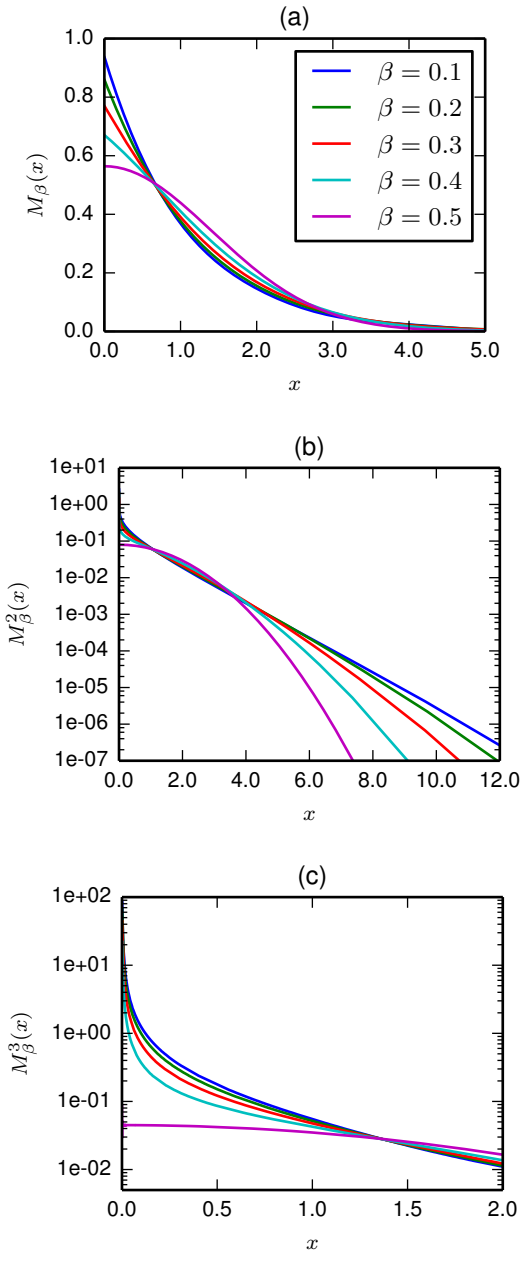

Figure 1: Fundamental solutions of the time-fractional diffusion equation (15) in the (a) one–dimensional, (b) two–dimensional and (c) three–dimensional cases for five values of the parameter β: $\beta = 0.1$, 0.2, 0.3, 0.4 and 0.5.

aim of investigating the effects of the parameter β on the short–term and long–term evolution of the random front.

In both cases, the computational domain is the rectangular region $[-2\,\mathrm{m}, 2\,\mathrm{m}]\times[-2\,\mathrm{m}, 2\,\mathrm{m}]$. The circular profile has a radius $r = 0.4\,\mathrm{m}$, and the square-shaped profile has a side ℓ such that in both cases the region enclosed by the front at $t = 0\,\mathrm{s}$ have the same surface (i.e. $\ell \approx 0.7\,\mathrm{m}$). The center of both the circular and square regions are located in $(x, y) = (0, 0)$.

In the first of the two above-mentioned scenarios, i.e. the one involving a circular initial front profile, when the diffusion coefficient ν is *small* enough, it is seen that for any of the values of the parameter β under investigation the only outstanding feature of the propagating front is its smoothing with respect to the sharp front characterizing the deterministic, i.e. non-diffusive, case. The profiles shown in Fig. 2, in which the numerically computed random fronts are plotted together with the deterministic front (dashed line) for the case $\nu = 10^{-3}\,\mathrm{m}^2\mathrm{s}^{-2\beta}$ and for two different values of the front velocity ($\mathcal{V} = 0.1\mathrm{ms}^{-1}$, $1\,\mathrm{ms}^{-1}$) at different time instants are representative of this behaviour. Moreover, as it is clearly seen from Figure 2(b,d,f), as the velocity of the front increases, the value of the parameter β becomes less and less relevant in terms of the propagating front profile, thus allowing to conclude that the knowledge of the exact value of β becomes less and less critical. On contrast, for smaller values of the front velocity, as shown in Figure 2(a,c,e), the front profile is clearly affected, at least qualitatively, by the value of the parameter β at any stage of the front evolution, being the profile sharper and sharper as the parameter β becomes smaller and smaller.

In Fig. 3 it is shown how the maximum value of the effective indicator φ_e, after being initially slightly affected by the diffusion processes, quickly recovers reaching again the initial maximum value.

From this analysis, it emerges that for *sufficiently small* values of the diffusion coefficient ν, the random front propagation differs from the deterministic front propagation merely for the shape of the front profiles as illustrated in

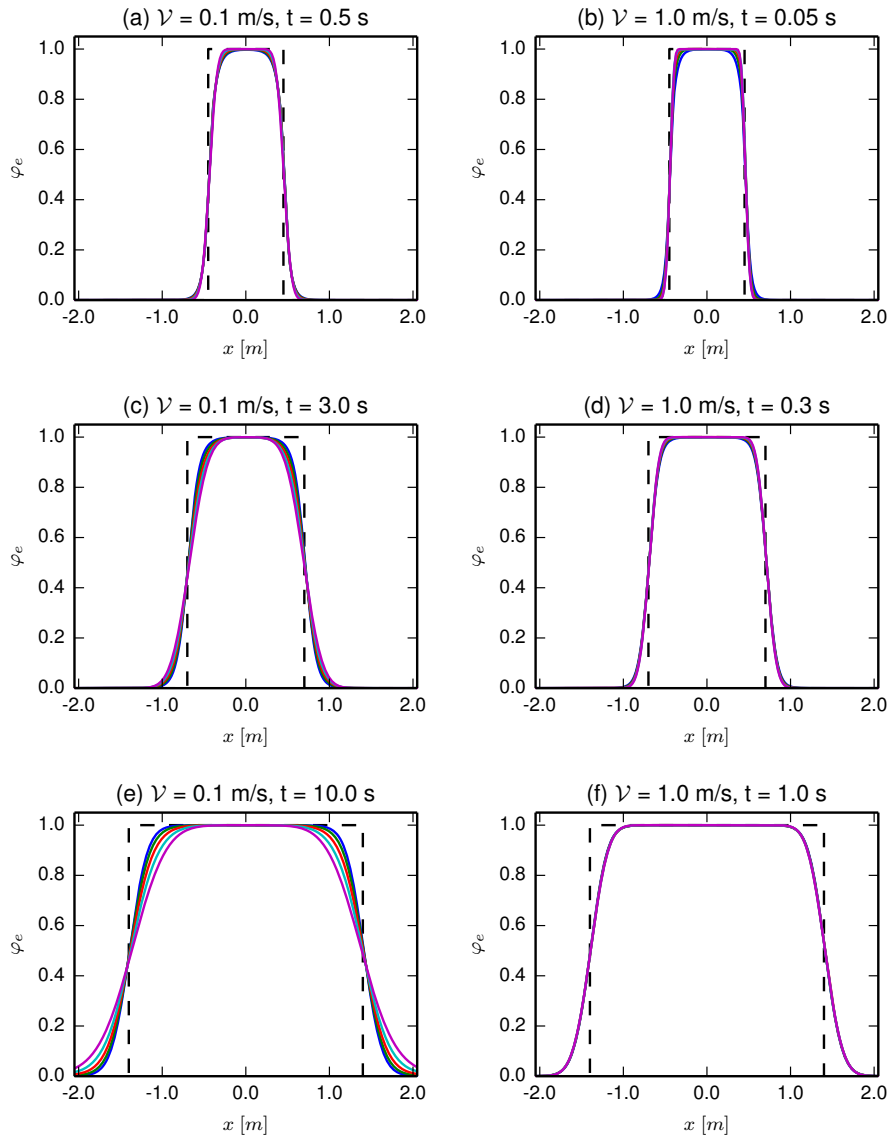

Figure 2: Cross-section at $y = 0$ of the φ_e fields corresponding to five values of the parameter β ($\beta = 0.1$, 0.2, 0.3, 0.4, 0.5) on the two-dimensional domain $[-2\,\mathrm{m}, 2\,\mathrm{m}] \times [-2\,\mathrm{m}, 2\,\mathrm{m}]$ at three values of the time t (top, middle and bottom row) and for two values of the front velocity (left and right column). The initial profile at $t = 0\,\mathrm{s}$ is circular, with centre $C = (0, 0)$ and radius $r = 0.4\,\mathrm{m}$. The diffusion coefficient is $\nu = 0.001\,\mathrm{m}^2\mathrm{s}^{-2\beta}$.

Fig. 2.

When the diffusion coefficient ν is *large*, the qualitative behaviour of the random fronts is remarkably different from the behaviour reported in Fig. 2 and Fig. 3. In fact, as it is shown in Fig. 4, in this case the smoothing of the front may reach the point as to affect the existence of the bulk of the region Ω_e enclosed by the propagating front, where the "bulk region" is intended as the region characterized by $\varphi_e = 1$. In this scenario, the maximum value of the effective indicator φ_e can be substantially reduced from its maximum unitary value, especially when the region Ω_e enclosed by the propagating front is small enough (i.e. for *small* times), leading to what may be referred to as a *weakening* effect of the diffusion phenomena on the region Ω_e. The comparison of the results obtained for two different values of the velocity of the front ($\mathcal{V} = 0.1\,\mathrm{ms}^{-1}$ and $\mathcal{V} = 1\,\mathrm{ms}^{-1}$, respectively shown in Fig. 4(a,c,e) and Fig. 4(b,d,f)), clearly put into evidence how the weakening effect described above is less relevant for the case with larger velocity.

For *large* times, as the region enclosed by the propagating front increases in size, the qualitative behaviour previously discussed for the case of a *small* diffusion parameter ν can be eventually recovered, as it is seen in Fig. 4(f) for the case with $\mathcal{V} = 1\,\mathrm{ms}^{-1}$. It is worth noting that for the case with $\mathcal{V} = 0.1\,\mathrm{ms}^{-1}$, the same behaviour takes place for time larger than that reported in Fig. 4(e), as can be argued from Fig. 5.

Figure 5 also puts into evidence how the *weakening* effect due to the diffusion process is largely dependent on the parameter β, as expected, as well as on the velocity $\mathcal{V}$ of the propagating front. In fact, the comparison of Fig. 5(a) and Fig. 5(b) shows how subdiffusive processes with *small* values of β may be responsible for smaller weakening effect with respect to subdiffusive processes with *larger* values of β (and also with respect to normal diffusive processes) when *small* values of the front velocity $\mathcal{V}$ are involved. Interestingly, the situation can be reversed when larger values of the front velocity are involved.

The features of the random fronts described so far for the case with $\nu =$

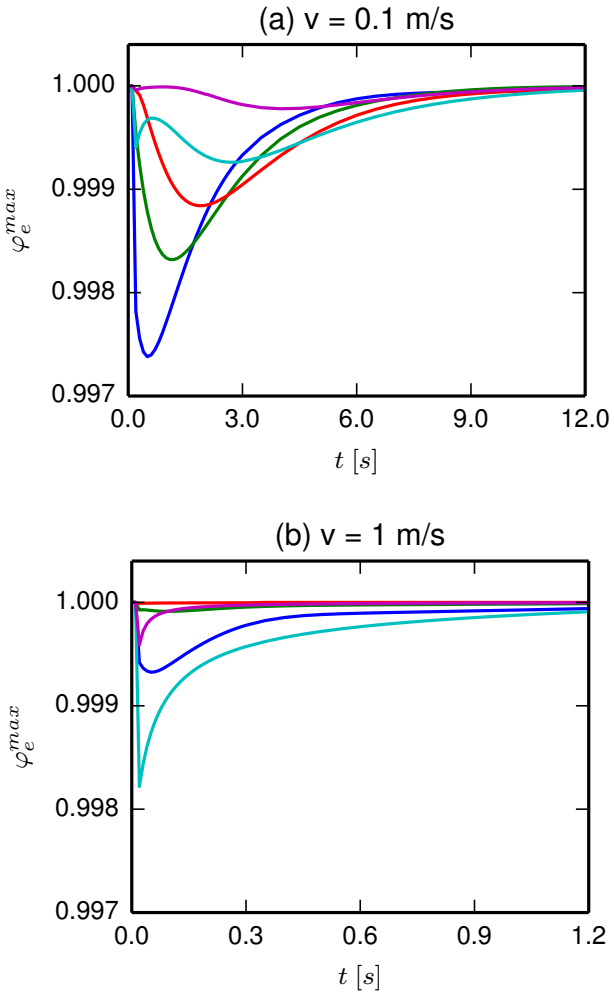

Figure 3: Time evolution of the maximum value of φ_e (φ_e^{max}) corresponding to five values of the parameter β ($\beta = 0.1$, 0.2, 0.3, 0.4, 0.5) for the case discussed in Figure 2.

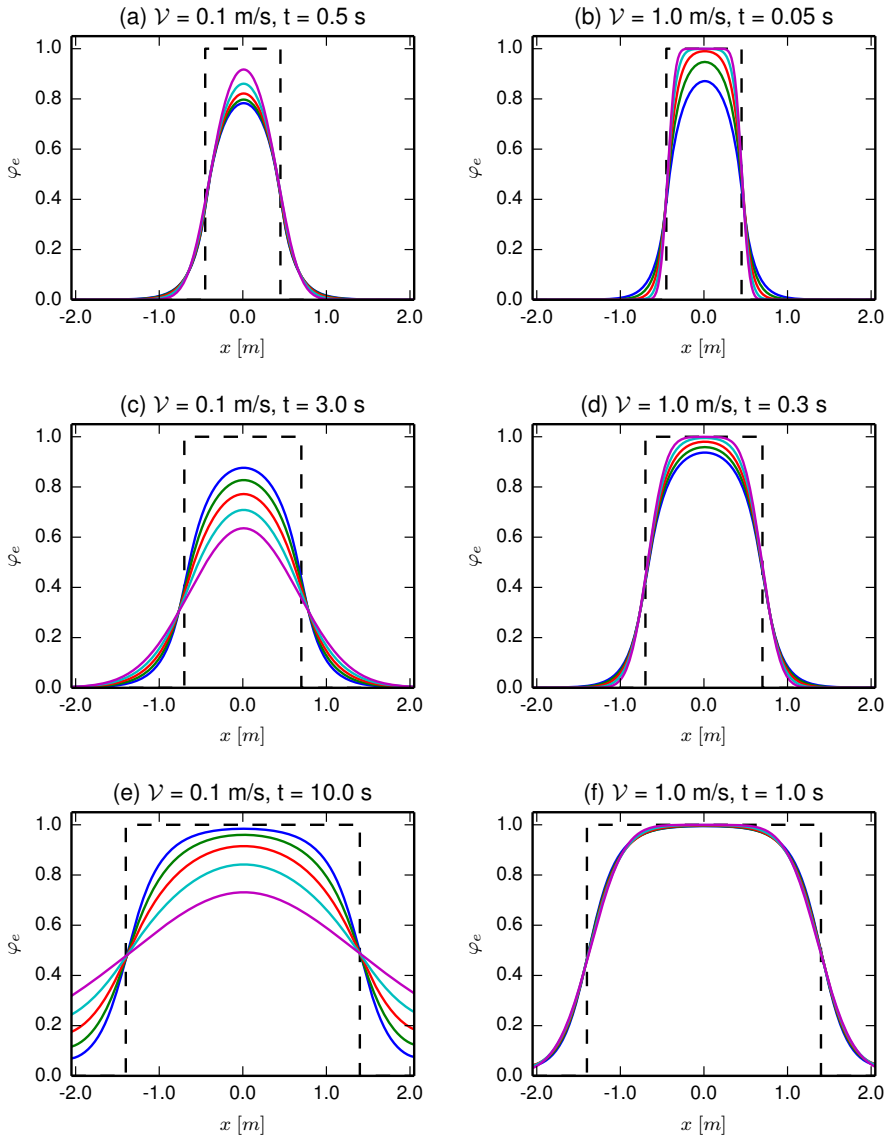

Figure 4: The same as in Figure 2 but with $\nu = 0.01\,\mathrm{m}^2\mathrm{s}^{-2\beta}$.

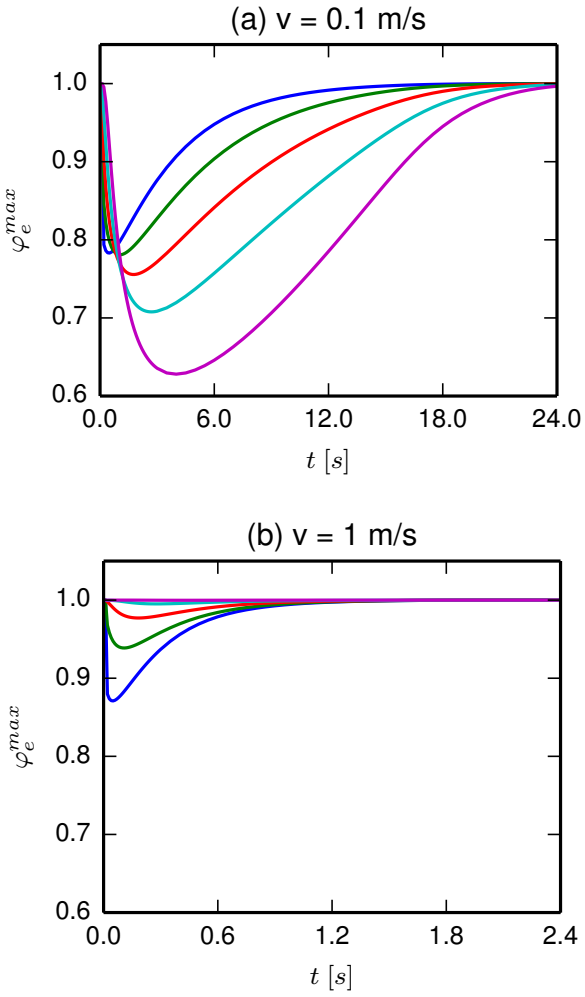

Figure 5: Time evolution of the maximum value of φ_e (φ_e^{max}) corresponding to five values of the parameter β ($\beta = 0.1$, 0.2, 0.3, 0.4, 0.5) for the case discussed in Figure 4.

$0.01\,\mathrm{m^2 s^{-2\beta}}$ remains qualitatively unchanged as the diffusion coefficient ν increases, but an important remark is in order. Depending on the physical interpretation of the indicator φ_e, it may – or may not – be meaningful to introduce the concept of "quencing" of the propagating front. In fact, assuming that the front is located, say, at the position for which the effective indicator φ_e reaches the threshold value φ_e^{th}, it might be meaningful to argue that when the effective indicator φ_e is reduced to the extent as to be less of φ_e^{th} over all the domain Ω_e, the region Ω_e extinguishes and no further front propagation takes place. Such a circumstance may, for instance, be the case met in the modelling of wildfire propagation [7]: if φ_e marks the position of the propagating front, the value of φ_e may drop below the given threshold value and the fire would be regarded as extinguished and no further calculation of the front evolution would be meaningful. Accordingly to what already noticed, such a circumstance would become more and more likely as the diffusion coefficient ν increases.

In Fig. 6, it is shown the propagation of the random and deterministic fronts obtained with $\nu = 0.1\,\mathrm{m^2 s^{-2\beta}}$. Assuming, for instance, $\varphi_e^{th} = 0.5$, area Ω_e associated with the front would be extinguished shortly after the diffusive process begins, independently from the value of the coefficient β (this is clearly seen also in Fig. 7), and any further calculation concerning the propagation of the connected random front would be meaningless, even if at larger times the effects of the diffusion would be such that the values of the effective indicator φ_e could reach values larger than the threshold φ_e^{th}, as it actually happens, as it is shown in Fig. 6(d,e,f) and Fig. 7. However, as already noticed, these considerations are problem-dependent and strongly connected with the physical process under consideration.

In order to investigate the two-dimensional effects connected to a non-axisymmetric initial front profile for various values of the parameter β, an initial square-shaped profile has been considered. The numerical results shown in Fig. 8, Fig. 9 and Fig. 10 correspond to diffusive processes characterized by $\beta = 0.1$, $\beta = 0.3$ and $\beta = 0.5$, respectively. Figures point out that at *small* times (i.e. $t < 1.0\,\mathrm{s}$)

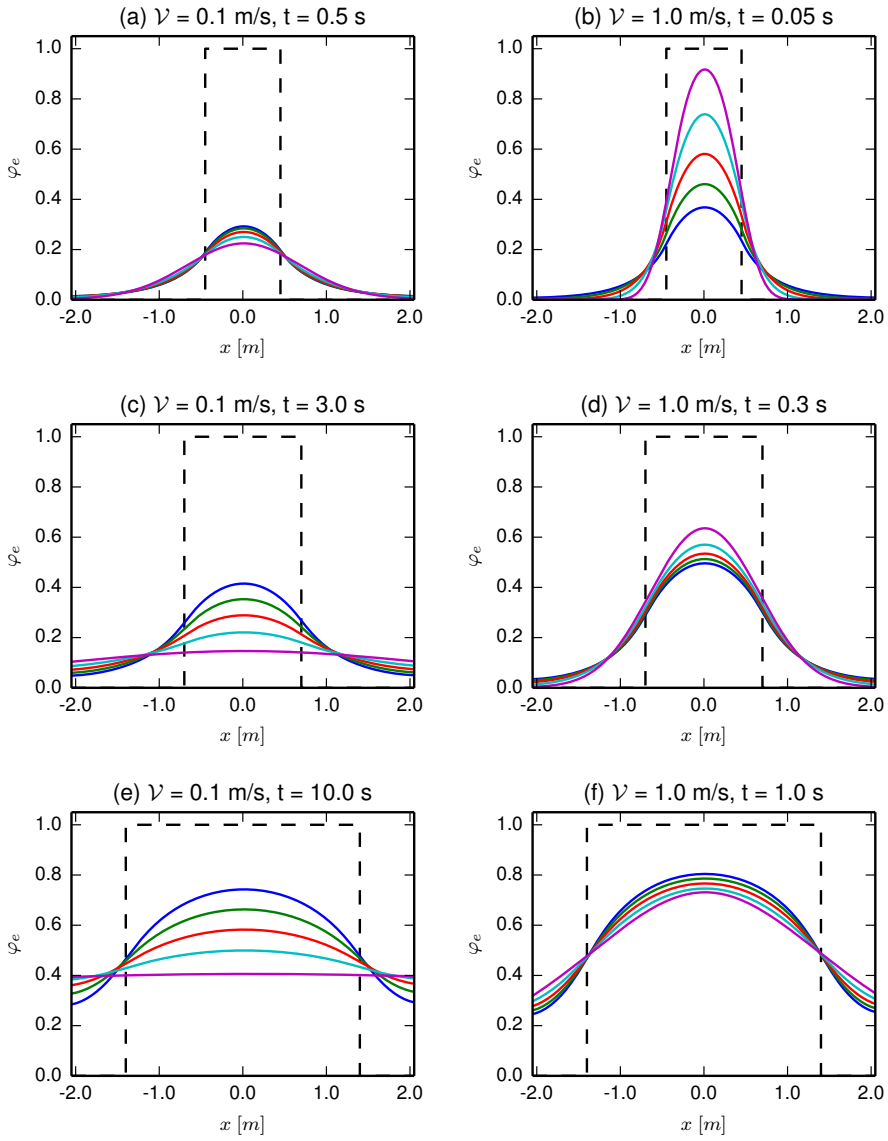

Figure 6: The same as in Figure 2 but with $\nu = 0.1\,\mathrm{m}^2\mathrm{s}^{-2\beta}$.

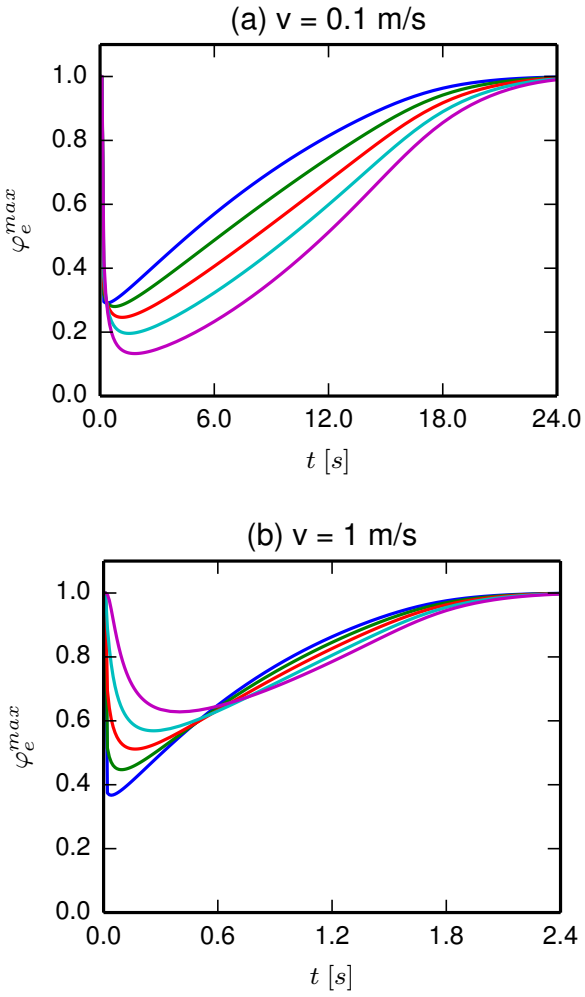

Figure 7: Time evolution of the maximum value of φ_e (φ_e^{max}) corresponding to five values of the parameter β ($\beta = 0.1$, 0.2, 0.3, 0.4, 0.5) for the case discussed in Figure 6.

when the value of β increases the effects of diffusion on the initial shape of the profile decreases, the subdiffusive process being in this case responsible for a stronger diffusive effects leading to a quicker smearing of the initial profile, because, when $t < 1.0\,\mathrm{s}$, the smaller the coefficient β the larger the particle variance (32). Among the three cases shown in Fig. 8, Fig. 9 and Fig. 10, the case characterized by the ordinary diffusion process is clearly the one in which the initial front profile remain almost unchanged for a longer time, being the profile also sharper. For large times – as seen in Fig. 8(d), Fig. 9(d) and Fig. 10(d) – the diffusion process leads to similar front profiles in all the discussed cases, being the effective indicator field φ_e undistinguishable, as a matter of fact, in all the three cases.

6. Conclusions

In this paper, a model for the study of the propagation of interfaces whose particles are subject to random motion due to anomalous diffusion phenomena is described, and numerical results for the case of fronts propagating in two–dimensional media are presented.

The model relies on the well-known LSM, which has proven in the past decades to be very successful in tracking the evolution of interfaces with complex motion. Since the LSM, in its traditional formulation, accounts only for the motion of deterministic interfaces (i.e. interfaces whose particles' motion is deterministic), the introduction of a suitable generalization capable of accounting for a random motion of the interface particles is in order [5]. This generalization is exploited in the case in which the PDF of the interface particle displacement is connected to the phenomena of anomalous diffusion.

The front propagation in presence of anomalous (and ordinary) diffusion is investigated with the aid of numerical calculations carried out by means of a suitably developed code and related library, and a selection of the computational results is presented focusing on a case with a circular initial front profile and on a case with a square-shaped initial front profile. In the first case, the investigation

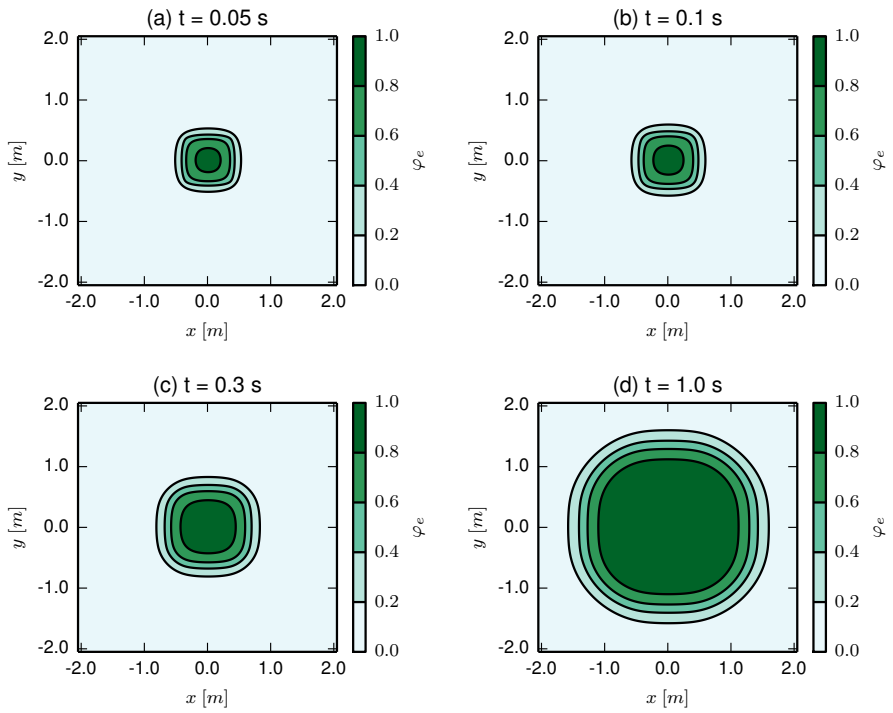

Figure 8: Distribution of the φ_e field for the case with $\beta = 0.1$ on the two-dimensional domain $[-2\,\mathrm{m}, 2\,\mathrm{m}] \times [-2\,\mathrm{m}, 2\,\mathrm{m}]$ at four instant times. The initial profile at $t = 0\,\mathrm{s}$ is a square, with center $C = (0, 0)$ and side $\ell = 0.7\,\mathrm{m}$. The diffusion coefficient is $\nu = 0.01\,\mathrm{m}^2\mathrm{s}^{-2\beta}$ and the front velocity is $\mathcal{V} = 1\,\mathrm{ms}^{-1}$.

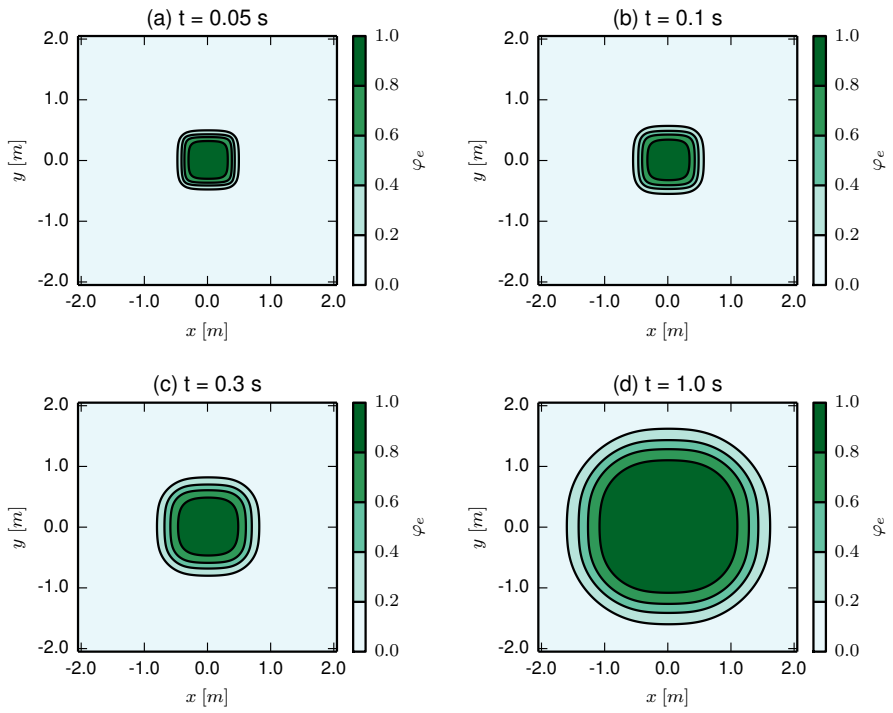

Figure 9: The same as in Figure 8 but for the case with $\beta = 0.3$.

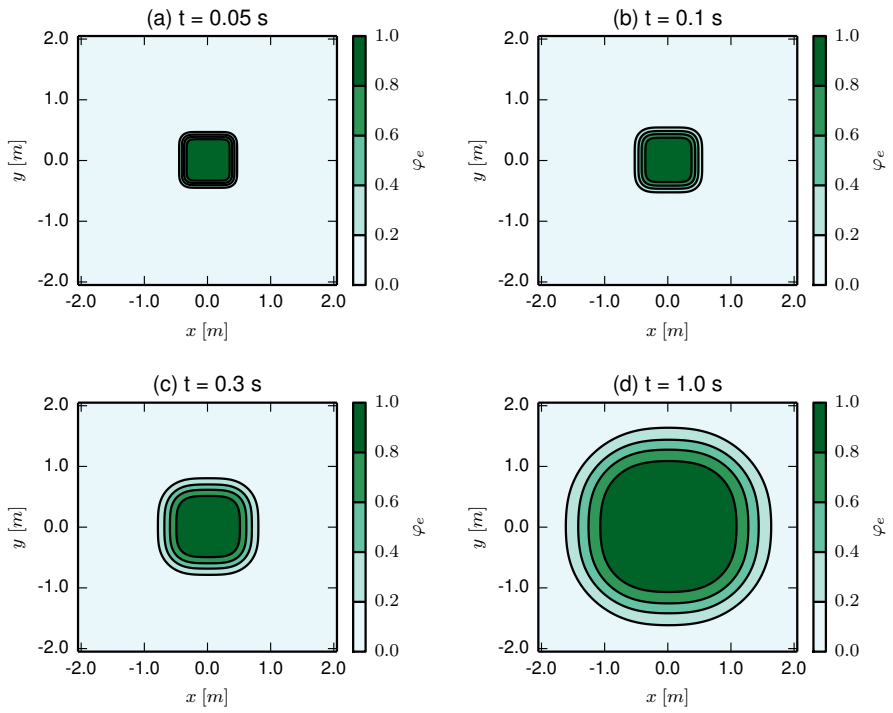

Figure 10: The same as in Figure 8 but for the case with $\beta = 0.5$.

is performed as to point out the effects on the random front propagation of the parameter β (which is half of the order of the time fractional derivative), the diffusion coefficient ν and the average front velocity $\mathcal{V}$. In the case of a square-shaped initial front profile, the primary intent of the investigation is to focus on the effects of the parameter β on the short-term and long-term evolution of the shape profile.

The presented numerical results clearly show that when the intensity of the diffusion (namely, the diffusion coefficient ν) is *small* enough, the propagating front is smoothed-out with respect to the sharp front obtained in the deterministic, i.e. non-diffusive case, but the overall qualitative behaviour of the front propagation is not affected by the diffusive phenomena taking place in the medium. On contrast, when the intensity of the diffusion is *large*, the qualitative behaviour of the random fronts sensibly changes: in this case the smoothing of the front may be so significant as to even compromise the existence of the region enclosed by the propagating front (and the front itself, in turn). This effect, which has been referred to as a *weakening* effect of the diffusion phenomena on the region bounded by the propagating front can be, as shown, a transient effect gradually vanishing as the front propagates, or even a phenomenon which drastically affects the very existence of the front, depending on the intensity of the diffusion itself. In both cases, it has been shown how the velocity of propagation of the front plays a significant role in the features of the front propagation, as the above-discussed *weakening* effect is reduced as the front velocity increases.

Moreover, aside from depending on the intensity of the diffusion phenomena through the diffusion coefficient ν, the above-mentioned *weakening* effects has also been shown to be more pronounced as the subdiffusive nature of the diffusion increases.

As far as the analysis of the propagation of an initially square-shaped front is concerned, it has been shown that, in the case under investigation and for *short* elapsed times (i.e. $t < 1.0\,\mathrm{s}$), small values of the parameter β leads to a smearing of the initial front shape remarkably faster than in the case of ordinary

diffusion. This occurs because, when $t < 1.0\,\mathrm{s}$, the smaller the coefficient β the larger the particle variance (32).

The LSM library utilized for the purpose of this investigation, featuring optimized FMM algorithms as well, is intended to be released as open source software under the GNU General Public License version 2 (GPLv2).

Acknowledgements

This work was developed in the framework of the Bizkaia Talent Grant AYD-000-226 *Combustion-wave interactions via extended thermodynamics* co-funded by Bizkaia Xede and European Commission (COFUND programme 2014/2016) and it has also been partially supported by GNFM/INdAM Young Researchers Project 2013 *Hyperbolic modelling into the extended thermodynamics framework to study combustion-wave interactions in turbulent premixed combustion*. GP would like to thank Prof. F. Mainardi for continuous support, suggestions and encouragement.

References

[1] A. Blumen, A. A. Gurtovenko, S. Jespersen, Anomalous diffusion and relaxation in macromolecular systems, J. Non-Cryst. Solids 305 (2002) 71–80.

[2] F. Höfling, T. Franosch, Anomalous transport in the crowded world of biological cells, Rep. Prog. Phys. 76 (2013) 046602.

[3] E. Barkai, Y. Garini, R. Metzler, Strange kinetics of single molecules in living cells, Phys. Today 65 (8) (2012) 29–35.

[4] G. Pagnini, Short note on the emergence of fractional kinetics, Physica A 409 (2014) 29–34.

[5] G. Pagnini, E. Bonomi, Lagrangian formulation of turbulent premixed combustion, Phys. Rev. Lett. 107 (2011) 044503.

[6] G. Pagnini, L. Massidda, The randomized level-set method to model turbulence effects in wildland fire propagation, in: D. Spano, V. Bacciu, M. Salis, C. Sirca (Eds.), Modelling Fire Behaviour and Risk. Proceedings of the International Conference on Fire Behaviour and Risk. ICFBR 2011, Alghero, Italy, October 4–6 2011, 2012, pp. 126–131, ISBN 978-88-904409-7-7.

[7] G. Pagnini, A. Mentrelli, Modelling wildland fire propagation by tracking random fronts, Nat. Hazards Earth Syst. Sci. Discuss. 1 (2013) 6521–6557.

[8] G. Pagnini, A model of wildland fire propagation including random effects by turbulence and fire spotting, in: Proceedings of XXIII Congreso de Ecuaciones Diferenciales y Aplicaciones XIII Congreso de Matemática Aplicada. Castelló, Spain, 9–13 September 2013, 2013, pp. 395–403.

[9] G. Pagnini, Fire spotting effects in wildland fire propagation, submitted.

[10] J. A. Sethian, P. Smereka, Level set methods for fluid interfaces, Ann. Rev. Fluid Mech. 35 (2003) 341–372.

[11] F. Mainardi, A. Mura, G. Pagnini, The M-Wright function in time-fractional diffusion processes: A tutorial survey, Int. J. Diff. Equations 2010 (2010) 104505.

[12] F. Mainardi, Fractional Calculus and Waves in Linear Viscoelasticity, Imperial College Press, London, 2010.

[13] G. Pagnini, The M-Wright function as a generalization of the Gaussian density for fractional diffusion processes, Fract. Calc. Appl. Anal. 16 (2) (2013) 436–453.

[14] F. Mainardi, G. Pagnini, R. Gorenflo, Mellin transform abd subordination laws in fractional diffusion processes, Fract. Calc. Appl. Anal. 6 (2003) 441–459.

[15] A. Hanyga, Multidimensional solutions of time-fractional diffusion-wave equations, Proc. R. Soc. Lond. A 458 (2002) 933–957.

[16] S. J. Osher, J. A. Sethian, Fronts propagating with curvature dependent speed: algorithms based on Hamilton–Jacobi formulations, J. Comput. Phys. 79 (1988) 12–49.

[17] N. Peters, Turbulent Combustion, Cambridge University Press, Cambridge, 2004.

[18] V. Mallet, D. E. Keyes, F. E. Fendell, Modeling wildland fire propagation with level set methods, Comput. Math. Appl. 57 (2009) 1089–1101.

[19] E. Jettestuen, J. O. Helland, M. Prodanović, A level set method for simulating capillary-controlled displacements at the pore scale with nonzero contact angles, Water Resour. Res. 49 (2013) 4645–4661.

[20] M. Machacek, G. Danuser, Morphodynamic profiling of protrusion phenotypes, Biophys. J. 90 (2006) 1439–1452.

[21] W. Guo, H. H. Sawin, Review of profile and roughening simulation in microelectronics plasma etching, J. Phys. D: Appl. Phys. 42 (2009) 194014.

[22] M. Oberlack, H. Wenzel, N. Peters, On symmetries and averaging of the g-equation for premixed combustion, Combust. Theory Modelling 5 (2001) 363–383.

[23] N. Peters, A spectral closure for premixed turbulent combustion in the flamelet regime, J. Fluid Mech. 242 (1992) 611–629.

[24] N. Peters, The turbulent burning velocity for large-scale and small-scale turbulence, J. Fluid Mech. 384 (1999) 107–132.

[25] A. N. Lipatnikov, V. A. S. V.A., Some basic issues of the averaged G-equation approach to premixed turbulent combustion modeling, Open Thermodyn. J. 2 (2008) 53–58.

[26] V. A. Sabel'nikov, A. N. Lipatnikov, Rigorous derivation of an unclosed mean G-equation for statistically 1D premixed turbulent flames, Int. J. Spray Combust. Dyn. 2 (2010) 301–324.

[27] J. J. Monaghan, Smoothed particle hydrodynamics, Rep. Prog. Phys. 68 (2005) 1703–1759.

[28] V. L. Zimont, Gas premixed combustion at high turbulence. turbulent flame closure combustion model, Exp. Therm. Fluid Sci. 21 (2000) 179–186.

[29] M. Kardar, G. Parisi, Y.-C. Zhang, Dynamic scaling of growing interfaces, Phys. Rev. Lett. 56 (1986) 889–892.

[30] V. A. Sabelnikov, A. N. Lipatnikov, Towards an extension of TFC model of premixed turbulent combustion, Flow Turbul. Combust. 90 (2013) 387–400.

[31] T. Ohta, D. Jasnow, K. Kawasaki, Universal scaling in the motion of random interfaces, Phys. Rev. Lett. 49 (1982) 1223–1226.

[32] H. M. Soner, N. Touzi, A stochastic representation for the level set equations, Commun. Part. Diff. Eq. 27 (2002) 2031–2053.

[33] O. Juan, R. Keriven, G. Postelnicu, Stochastic motion and the Level Set Method in Computer Vision: Stochastic active contours, Int. J. Comput. Vision 69 (2006) 7–25.

[34] A. Mentrelli, G. Pagnini, Random front propagation in fractional diffusive systems, submitted.

[35] Y. L. Klimontovich, Nonlinear Brownian motion, Physics-Uspekhi 37 (1994) 737–767.

[36] W. R. Schneider, W. Wyss, Fractional diffusion and wave equations, J. Math. Phys. 30 (1) (1989) 134–144.

[37] F. Mainardi, Fractional relaxation-oscillation and fractional diffusion-wave phenomena, Chaos Solitons Fract. 7 (1996) 1461–1477.

[38] F. Mainardi, The fundamental solutions for the fractional diffusion-wave equation, Appl. Math. Lett. 9 (6) (1996) 23–28.

[39] F. Mainardi, Y. Luchko, G. Pagnini, The fundamental solution of the space-time fractional diffusion equation, Fract. Calc. Appl. Anal. 4 (2) (2001) 153–192.

[40] F. Mainardi, G. Pagnini, The Wright functions as solutions of the time-fractional diffusion equation, Appl. Math. Comput. 141 (1) (2003) 51–62.

[41] F. Mainardi, G. Pagnini, R. Gorenflo, Some aspects of fractional diffusion equations of single and distributed order, Appl. Math. Comput. 187 (2007) 295–305.

[42] F. Mainardi, R. Gorenflo, On Mittag–Leffler-type functions in fractional evolution processes, J. Comput. Appl. Math. 118 (2000) 283–299.

[43] A. Mentrelli, liblsm90: An open source library for level set and fast marching methods (2014–).
URL `http://mentrelli.it/liblsm90`

[44] R. Gorenflo, J. Loutchko, Y. Luchko, Computation of the Mittag–Leffler function $E_{\alpha,\beta}(z)$ and its derivative, Fract. Calc. Appl. Anal. 5 (2002) 491–518.

[45] E. Jones, T. Oliphant, P. Peterson, et al., SciPy: Open source scientific tools for Python (2001–).
URL `http://www.scipy.org/`

[46] J. D. Hunter, Matplotlib: A 2D graphics environment, Comput. Sci. Eng. 9 (3) (2007) 90–95.

[47] F. Pérez, B. E. Granger, IPython: a system for interactive scientific computing, Comput. Sci. Eng. 9 (3) (2007) 21–29. `doi:10.1109/MCSE.2007.53`.
URL `http://ipython.org`